# Synthesis and spectroscopy of Co-II, Ni-II, Cu-II and Zn-II complexes derived from 3,5-disubstituted-1H-pyrazole derivative: A special emphasis on DNA binding and cleavage studies

**ARTICLE** *in* EUROPEAN JOURNAL OF MEDICINAL CHEMISTRY · OCTOBER 2009

Impact Factor: 3.45 · DOI: 10.1016/j.ejmech.2009.10.026 · Source: PubMed



**5 AUTHORS**, INCLUDING:

Srinivasa Budagumpi
Jain University
**60** PUBLICATIONS **602** CITATIONS
SEE PROFILE

Naveen V. Kulkarni
University of Texas at Arlington
**31** PUBLICATIONS **197** CITATIONS
SEE PROFILE

Vidyanand Revankar
Karnatak University, Dharwad
**67** PUBLICATIONS **595** CITATIONS
SEE PROFILE

European Journal of Medicinal Chemistry 45 (2010) 455–462

Contents lists available at ScienceDirect

European Journal of Medicinal Chemistry

journal homepage: http://www.elsevier.com/locate/ejmech

Original article

# Synthesis and spectroscopy of $Co^{II}$, $Ni^{II}$, $Cu^{II}$ and $Zn^{II}$ complexes derived from 3,5-disubstituted-1*H*-pyrazole derivative: A special emphasis on DNA binding and cleavage studies

Srinivasa Budagumpi, Naveen V. Kulkarni, Gurunath S. Kurdekar, M.P. Sathisha, Vidyanand K. Revankar*

*Department of Studies in Chemistry, Karnatak University, Pavatenagar, Dharwad 580 003, Karnataka, India*

ARTICLE INFO

*Article history:*
Received 25 July 2009
Received in revised form
10 October 2009
Accepted 15 October 2009
Available online 28 October 2009

*Keywords:*
3,5-Dichloroformyl-1*H*-pyrazole
Quinoxaline
Gel-electrophoresis
DNA
Biogram

ABSTRACT

A series of novel $Co^{II}$, $Ni^{II}$, $Cu^{II}$ and $Zn^{II}$ complexes of 1*H*-pyrazole-3,5-dicarboxylic(2′-hydroxy-3′-hydrazinequinoxaline) has been prepared and characterized by the spectral and analytical techniques. $Cu^{II}$ ion reacts with the ligand $LH_3$ and forms the complex in one compartment of the ligand whereas, the other compartment remains free. In $Co^{II}$, $Ni^{II}$ and $Zn^{II}$ complexes both compartments of $LH_3$ are involved in the coordination. DNA binding/cleavage studies were revealed the stronger binding capability of the present $Ni^{II}$ complex, confirmed by the absorbance, viscometric and gel-electrophoresis studies. Similarly, remaining complexes do the same in the ligand field with lesser binding constants, subsequently, no complex was found to cleave the DNA. Finally, $Cu^{II}$ complex shows growth inhibitory activity against biogram.



## 1. Introduction

Stable, inert, and non-toxic metal complexes containing spectroscopically active metal centers are exceptionally valuable as probes of biological systems. Transition metal complexes of pyrazole derivatives have been the subject of much recent notice because of their beneficial effects as anticancer agents [1–3]. A large body of evidences indicate the mechanism of action of anticancer agents binds through distinctive binding modes to the DNA of cancer infected cell in such a way, that the cell cannot replicate further, this inhibition of replication finally leads to the death of the infected cell. The binding modes are responsible for activity and the mechanism by which DNA replication is totally inhibited in cancer cells. The classical coordination complex of platinum, *iproplatin* is biologically more active especially as antitumor drug because of its structural features, which leads to the formation of sequence-specific adducts between *iproplatin* and DNA, which eventually provide the clues for binding modes with DNA. A more complete understanding of how to target DNA sites with specificity, size and shape will lead not only to novel chemotherapeutics but also to a greatly expanded ability for chemists to probe DNA and to develop highly sensitive and appropriate diagnostic agents.

In coordination chemistry point of view, pyrazole is an important class of organic compounds with two nitrogen atoms as hetero atoms attached neighboring to each other. Both the nitrogen atoms can strongly coordinate to the two metal centers by deprotonation; hence can act as endogenous bridge between the metal ions and preferably form binucleating metal complexes [4–6]. Some of the 3,5-disubstituted pyrazole derivatives can be converted in to macroacyclic and macrocyclic compounds as well [7,8] further these acts as polydentate chelates and form the stable coordination compounds of transition metal ions with greater specificity. The diazine bridge and the aided potential donor groups like hydrazide –NH and phenolic –OH at 3- and 5- positions are the interesting structural peculiarities for designing the ligand which are as same as in *iproplatin*. Hence the complexes derived from this type of ligand systems are expected to bind with DNA as *iproplatin* can do. In this connection, we have prepared a series of transition metal complexes and investigated their DNA binding activity. In the present research article we wish to report the synthesis, structure, redox properties, anti-biogram and DNA binding and cleavage studies of transition metal complexes of 3,5-disubstituted pyrazole derivative.

* Corresponding author. Tel.: +91 836 4250821, +91 09900485652 (mobile).
*E-mail address:* vkrevankar@rediffmail.com (V.K. Revankar).

0223-5234/$ – see front matter © 2009 Elsevier Masson SAS. All rights reserved.
doi:10.1016/j.ejmech.2009.10.026

## 2. Results and discussion

### 2.1. Chemistry

The analytical and physicochemical data of the complexes are summarized in Table 1. All complexes are soluble in organic solvents like DMF, DMSO and acetonitrile.

#### 2.1.1. Infrared spectral studies

The IR spectral details are shown in Table 2. IR spectrum of ligand shows a strong band at 1653 $cm^{-1}$, assigned to amide carbonyl (>C═O) [9], remains unchanged on complexation suggesting its non-involvement in the coordination. Broad band at 3447 $cm^{-1}$ shows the presence of hydroxyl (–OH) groups of quinoxaline moiety, which on complexation disappears and could be due to coordination of oxygen to metal ions after deprotonation. Intense bands at 3174, 3045 and 3000 $cm^{-1}$ in ligand are attributed to hydrazide N–H, amide N–H and pyrazole ring N–H respectively [9]. In complexes, hydrazide N–H shifts to the lower region which suggests the coordination of hydrazide nitrogen and the same was further supported by the $^1$H NMR spectrum of the $Zn^{II}$ complex.

In case of $Co^{II}$, $Ni^{II}$ and $Zn^{II}$ complexes a new band appeared in the region 1520–1535 $cm^{-1}$ and the same was assigned to the formation of new >C═N bond in pyrazole ring which is less than that of the normal >C═N in pyrazole [10]. This observation supports the coordination of both the nitrogen atoms of the pyrazole moiety to the metal centers. In $Cu^{II}$ complex, the sharp splitting of bands at 1528, 1503 $cm^{-1}$ and 3054, 3044 $cm^{-1}$ suggests that, the coordination occurs at one side of the ligand as shown in the Fig. 4. $Co^{II}$ and $Ni^{II}$ complexes show a sharp band at 3419 and 3426 $cm^{-1}$ which are due to the presence of –OH as exogenous bridging unit between metal centers [11].

#### 2.1.2. $^1$H NMR spectral studies

$^1$H NMR spectrum of the ligand and its $Zn^{II}$ complex was scanned in the range 0–16 $\delta$ ppm. The ligand displayed the signals at 14.1, 11.9, 10.9 and 4.3 $\delta$ ppm which can be attributed to N–H of pyrazole ring [12], –OH proton of quinoxaline, amide protons and hydrazide protons respectively. In addition to this, a set of multiplet was observed in the range 6.96–7.85 $\delta$ ppm due to the presence of aromatic protons.

The comparative study of $^1$H NMR data of ligand and its zinc complex reveals about the ligational behavior of the ligand. In the $^1$H NMR spectrum of zinc complex, the signals due to pyrazole N–H and quinoxaline –OH protons were absent indicating the involvement of both the nitrogen atoms of pyrazole ring and oxygen atoms of quinoxaline in the coordination after deprotonation respectively. Further hydrazide N–H peak is shifted to 3.4 $\delta$ ppm, which suggests the coordination of nitrogen atoms and there is no significant changes in the remaining peaks including in their intensities.

#### 2.1.3. UV–visible spectral studies

UV-visible spectral data of the ligand and its complexes are tabulated in Table 3. The electronic spectra of ligand and complexes were recorded in DMF solution in the scan range 200–1000 nm. Ligand exhibits a band at 277 nm, due to the intra-ligand $\pi \rightarrow \pi^*$ transition, which remains unchanged in all the complexes. The shoulder at 390 nm in ligand is assigned for $n \rightarrow \pi^*$ transition of >N–H group [13]. This band is not found in complexes, suggesting the coordination of nitrogen atoms. A shoulder at 425 nm was assigned to $n \rightarrow \pi^*$ transition originating from the amide functions [13].

Electronic spectrum of cobalt complex shows an asymmetric band at 623 nm, assigned to d–d transition, and a sharp charge transfer band at 410 nm, which is in consistent with the tetrahedral geometry [13,14]. Nickel complex displays two distinct bands at 575 and 615 nm which are assigned as d–d transitions and a sharp charge transfer transition occurs at 330 nm, collectively all these offers the square pyramidal geometry [15]. Electronic spectrum of copper complex exhibits charge transfer transition at 360 nm and a broad band in the region 475–530 nm corresponds to the d–d transition. Such broad asymmetric bands near 550 nm have been observed for related copper complexes with square pyramidal geometry [16,17]. Finally, the spectrum of zinc complex shows band in the range 426–453 nm is accounted for the ligand to metal charge transfer transition.

#### 2.1.4. Magnetic properties

Magnetic moment data of the complexes were recorded at room temperature and are shown in Table 1. Copper complex shows the effective magnetic moment $\mu_{eff}$ 1.62 B.M., which is less than that of the spin only value (1.73 BM) and attributed to the weak antiferromagnetic interaction between copper centers through the bridged quinoxaline oxygen atoms. Thus the magnetic moment value and spectral data supports the square pyramidal geometry for the complex. In addition to this, the magnetic moments of nickel and cobalt complexes were found to be 2.82 and 4.05 BM respectively supporting the assigned geometry. These magnetic moment values are almost same as spin only values of $Co^{II}$ and $Ni^{II}$ free ions respectively. The lower magnetic moment values are due to the very weak antiferromagnetic interaction between metal centers through the exogenous –OH bridge. These magnetic moment value and spectral data confirms the square pyramidal [18] and tetrahedral [19] geometries around nickel and cobalt ions respectively.

#### 2.1.5. ESR spectral study

The powder state ESR spectrum of copper complex was operated in the region 9000 MHz with corresponding field intensity at ~3000 Gauss at room temperature. The spectrum exhibits isotropic intense broad signal with $g_{iso}$ 2.072 and no hyperfine splitting was observed. ESR spectrum of this kind have been reported earlier for complexes having large organic ligands [20], and also the broad ESR signal indicates the presence of chloro coordinated binuclear copper(II) complexes [21]. This broadening is because of the dipolar interaction.

#### 2.1.6. Molar conductivity measurements

The molar conductance value of complexes was obtained at room temperature in DMF solution with $10^{-3}$ mol/$dm^3$

**Table 1**
Analytical, magnetic moment and conductance data of $Co^{II}$, $Ni^{II}$, $Cu^{II}$ and $Zn^{II}$ complexes.[a]

| Sl. No | Complex | Metal | Carbon | Hydrogen | Nitrogen | Chloride | $\mu_{eff}$ in BM | Molar conductance mho $cm^2$ $mole^{-1}$ |
|---|---|---|---|---|---|---|---|---|
| 1) | $[Co_2L(OH)]\cdot 3H_2O$ | 17.45 (16.92) | 32.27 (32.86) | 3.25 (3.01) | 20.71 (21.09) | 5.71 (5.78) | 4.05 | 3.5 |
| 2) | $[Ni_2LCl(H_2O)_2]\cdot 2H_2O$ | 17.00 (17.62) | 36.31 (36.98) | 3.45 (4.01) | 20.17 (20.91) | 5.04 (5.44) | 2.82 | 3.8 |
| 3) | $[CuLH_2Cl]_2\cdot 4H_2O$ | 10.49 (11.11) | 41.65 (41.02) | 2.97 (3.09) | 23.14 (23.72) | 5.78 (5.01) | 1.62 | 3.3 |
| 4) | $[Zn_2L(OH)]\cdot 3H_2O$ | 19.10 (20.01) | 36.46 (35.94) | 2.31 (2.40) | 20.26 (20.91) | 5.06 (5.70) | – | 2.4 |

[a] Calculated values are given the parenthesis.

**Table 2**
Infrared spectral data of ligand and complexes b: Broad band; s: Sharp band.

| Compounds | >C = O (amide) | N–H (hydrazide) | N–H (pyrazole) | –OH (quinoxaline) | >C = N (pyrazole) | M-N | –OH (bridge) |
|---|---|---|---|---|---|---|---|
| $LH_3$ | 1656 | 3219 | 3045 | b 3447 | 1565 | – | – |
| $[Co_2L(OH)]\cdot 3H_2O$ | 1653 | ~3150 | – | – | 1520 | 472 | s 3419 |
| $[Ni_2LCl(H_2O)_2]\cdot 2H_2O$ | 1648 | ~3100 | – | – | 1531 | 475 | s 3426 |
| $[CuLH_2Cl]_2\cdot 4H_2O$ | 1657 | ~3200 | 3044 | b 3435 | 1531 | 476 | – |
| $[Zn_2L(OH)]\cdot 3H_2O$ | 1661 | ~3100 | – | – | 1535 | 473 | – |

concentration. The molar conductivity values of all the complexes fall in the range 2.4–3.8 ohm $cm^2$ $mol^{-1}$ (shown in Table 1), which is in agreement with non-electrolytic nature of the complexes [22].

### 2.1.7. FAB mass spectral studies

The elemental and analytical data of the copper complex suggests the empirical formula $[CuLH_2Cl]_2.4H_2O$ and this is supported by the FAB mass spectrum. The peaks at highest *m*/*z* value cannot always be assigned with certainty, but the isotopic pattern is consistent with a binuclear complex. A peak at *m*/*z* 1216 was observed, corresponding to the mass of the entire mononuclear, dimeric complex including coordinated chloride ion and lattice celled water molecules [23]. Apart from this, spectrum shows some other peaks, which are due to molecular cations of various fragments of complex. By comparing all the analytical and spectral data of cobalt, nickel and zinc complexes, it is evident that these are monomeric and binuclear complexes.

### 2.1.8. Thermal studies

The thermogravimetric analysis of the $Cu^{II}$ complex has been carried out in nitrogen environment over the temperature range 30–1000 °C. TG curves of copper complex show weight losses in three considerable steps. In the first step 4.7%, in the temperature range 55–120 °C attributed to the weight loss of four lattice celled water molecules and this process is endothermic in nature, which is evident by the DTA signal at 98 °C. The weight loss at second step is 15.25% observed in the temperature range 130–280 °C which may be due to combined elimination of chloride as HCl and some part of the ligand, the corresponding DTA signal is at 201 °C. Partially decomposed complexes are unstable and decompose completely in the next step means, the remaining part of the ligand is completely eliminated in third stage of weight loss in the temperature range 280–520 °C, and thereafter the curve became plateau due to the formation of stable CuO.

### 2.1.9. Cyclic voltammetric studies

The cyclic voltammograms of ligand and copper complex were recorded at room temperature in DMF solution under oxygen free conditions, which was created by purging pure nitrogen gas. An assembly of three electrodes consists of glassy carbon working electrode, a platinum auxiliary electrode and Ag/AgCl reference electrode was used and tetramethyl ammonium chloride with 0.1 M concentration as supporting electrolyte.

**Table 3**
UV–visible spectral data of ligand and complexes.

| Compounds | Peak values (in nm) ($\lambda_{max}$ in $cm^{-1}$) |
|---|---|
| $LH_3$ | 430 (23,256), 390 (25,641), 277 (36,101) |
| $[Co_2L(OH)]\cdot 3H_2O$ | 623–600 (16,051–16,667), 421 (23,753), 342 (29,250), 311 (32,154), 275 (36,364) |
| $[Ni_2LCl(H_2O)_2]\cdot 2H_2O$ | 615 (16,260), 575 (17,391), 330 (30,303), 340 (29,412), 320 (31,250), 311 (32,154) |
| $[CuLH_2Cl]_2\cdot 4H_2O$ | 476–530 (21,008–18,868), 360 (27,778), 325 (30,769), 310 (32,258) |
| $[Zn_2L(OH)]\cdot 3H_2O$ | 453 (22,075), 426 (23,474), 400 (25,000), 275 (36,364) |

The cyclic voltammogram of ligand and copper complex were scanned in the potential range of +1.0 to −1.0 V with different scan rates viz., 0.05, 0.1 and 0.15 V/s. Ligand did not show any electrochemical response over the working potential range. The cyclic voltammogram of copper complex is shown in Fig. 1. The voltammogram shows one electron transfer process in anodic potential scan, with oxidation peak at 0.31, 0.33 and 0.34 V at above mentioned scan rates and the same is attributed to the oxidation of $Cu^{II} \rightarrow Cu^{III}$. After the oxidation peak, cathodic peaks were observed at 0.12, 0.14, 0.15 V and −0.36, −0.37, −0.39 V during cathodic scan at above mentioned scan rates and were assigned to the reduction of $Cu^{III} \rightarrow Cu^{II}$ and finally $Cu^{II} \rightarrow Cu^{I}$ [12]. It is concluded from cyclic voltammetric studies that, the copper complex exhibits one-electron transfer process in anodic scan and two-electron transfer process in cathodic scan. The separation between anodic and the first cathodic peak potentials i.e., ΔEp = Epa − Epc is 192 mV indicates the quasireversible redox process.

## 2.2. Biochemistry

### 2.2.1. Anti-biogram analysis

In order to study the comparative biological activities, the compounds were screened for antibacterial (against *Escherichia coli*, *Aeruginosa Pseudomonasa*) and antifungal (against *Aspergillus Niger*, *Cladosporium*) activities at 500 μg and 250 μg concentrations in DMF, out of which the later was treated as minimum inhibitory concentration (MIC).

The copper complex shows moderate activity i.e. 43.75 and 41.37% zone of inhibition against *E. coli*, *A. Pseudomonasa* bacteria respectively at 500 μg concentration, which is more than that of ligand activity. In MIC level, only copper complex is active against *A. Pseudomonasa* with 12.5% zone of inhibition. In antifungal studies, copper complex exhibits extremely high activity, 100% zone of inhibition, against *A. Niger* which is as good as the internal standard at both the concentrations. The moderate activity, 77.7 and 33.3%, at both the concentration levels was shown against *Cladosporium.*

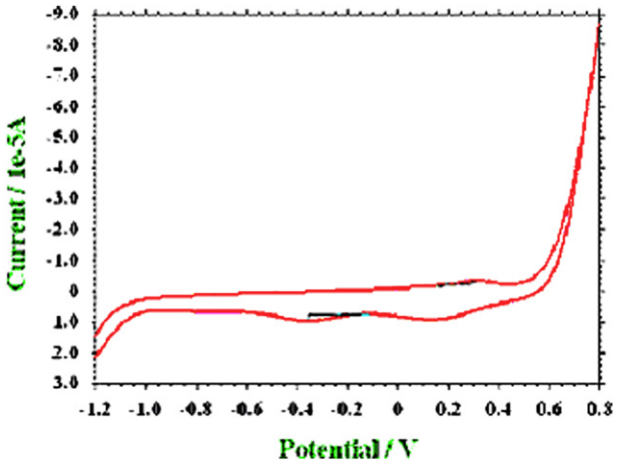


**Fig. 1.** Cyclic voltammogram of copper (II) complex at scan rate of 0.1 V $s^{-1}$.

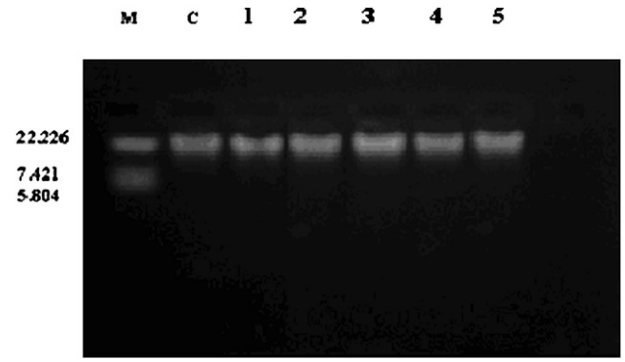


**Fig. 2.** Gel-electrophoresis picture of ligand and its complexes. Photograph showing the effects of transition metal complexes on DNA of *E. Coli.* Lane M: DNA marker, Lane C: Untreated DNA, Lane 1: Ligand ($LH_3$), Lane 2: $[Co_2Lm(OH)]$, Lane 3: $[Ni_2Lm(Cl)(H_2O)_2]$, Lane 4: $[Cu_2(LH_2Cl)_2].4H_2O$, Lane 5: $[Zn_2Lm(OH)]$.

### 2.2.2. DNA cleavage studies by gel-electrophoresis method

Gel-electrophoresis technique works on the migration of DNA under the influence of electric potential. Gel-electrophoresis picture is shown in Fig. 2. The photograph shows the bands with different bandwidth, compared to the control, is the differentiating criteria for binding ability of complexes with *E. coli* in this study. Control experiment using DNA alone does not show any significant cleavage of DNA even after a longer exposure time. In lanes 2–4, width of the DNA band is little bigger and intense in appearance and shows tailing to a very lesser extent. This result revealed the stronger binding of the complexes to DNA in $[Co_2L(OH)]$, $[Ni_2L(Cl)(H_2O)_2]$, and $[Cu_2(LH_2Cl)_2]\cdot 4H_2O$ systems and could be attributed to the binding but not the cleavage. On the other hand, lanes 1 and 5 do not show any significant changes even in the intensity and bandwidth compared to the control which elucidates the inactiveness of ligand and $[Zn_2L(OH)]$ complex towards the binding or cleavage of *E. Coli* DNA.

### 2.2.3. DNA binding analysis using electronic spectral method

The UV–visible spectral technique is the most commonly used method to know the interaction of metal complexes with DNA [24–26], since transition metal complexes often have abundant spectroscopic properties. The representative absorption spectrum of $Ni^{II}$ complex in presence/absence of *E. Coli* DNA is shown in the Fig. 3. The binding behavior of complexes to *E. coli* DNA helix has been followed through absorption spectral titrations. With increasing concentration of *E. coli* DNA, the absorption bands of the complexes were affected, resulting in the tendency of hypochromism and a remarkable red shift is observed in all the complexes. There are two isosbestic points observed for all the four complexes. This implies that 1: 1 complex: DNA stoichiometry is maintained during the binding process and/or there is only one

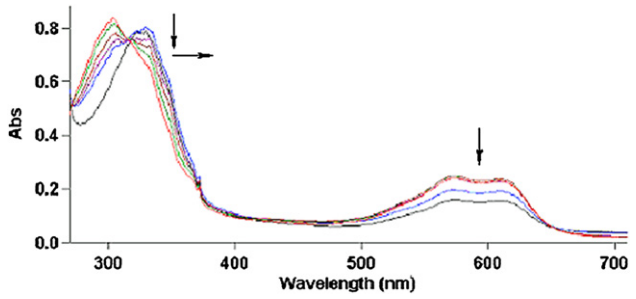


**Fig. 3.** Absorption spectra $[Ni_2L\mu(Cl)(H_2O)_2]$ in the absence (very first line from pinnacle) and in the presence of increasing amounts of *E. coli* DNA. Arrow mark shows the absorption changes upon changing the *E. coli* DNA concentration.

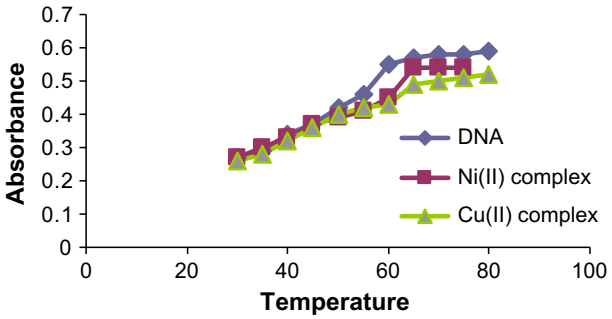


**Fig. 4.** Effects of increasing temperature on *E. coli* DNA alone, *E. coli* DNA with Ni-complex and Cu-complex.

type of binding of the complexes to DNA is found. With decrease in the absorbance and appreciable red shift of the absorption maximum at around 330 nm in all the complexes (the shift being 11, 23, 17 and 14 nm for $[Co_2L(OH)]\cdot 3H_2O$, $[Ni_2LCl(H_2O)_2]\cdot 2H_2O$, $[CuLH_2Cl]_2\cdot 4H_2O$ and $[Zn_2L(OH)]\cdot 3H_2O$ respectively) indicates the intercalation. The binding constants of the complexes $[Co_2L(OH)]\cdot 3H_2O$, $[Ni_2LCl(H_2O)_2]\cdot 2H_2O$, $[CuLH_2Cl]_2\cdot 4H_2O$ and $[Zn_2L(OH)]\cdot 3H_2O$ are found to be $6.1\times10^4$, $1.34\times10^6$, $1.87\times10^5$ and $3.25\times10^5$ respectively.

### 2.2.4. DNA melting temperature ($T_m$) studies

The $T_m$ of *E. coli* DNA is the temperature at which 50% of the nucleotide and its perfect complement are in duplex. Typically, annealing or hybridizations are performed at 5–10 °C below the $T_m$ of a duplex. Stability of the DNA double helix influences the melting temperature ($T_m$) of DNA, while the binding of compounds to DNA alters the $T_m$ depending on the strength of interactions. The intercalation of the complexes into the DNA base pairs causes stabilization of base stacking and hence raises the melting temperature of the double stranded DNA. The DNA melting experiment is useful in establishing the extent of intercalation [27]. As shown in Fig. 4, the $T_m$ of DNA in the absence of any added complex was found to be $58\pm1$ °C, under our experimental conditions [28]. Under the same set of conditions, the presence of $[CuLH_2Cl]_2\cdot 4H_2O$ and $[Ni_2LCl(H_2O)_2]\cdot 2H_2O$ complexes increased the $T_m$ of about 3 and 6 °C respectively, which is characteristic of an intercalative binding behavior of the complexes with the DNA [29].

### 2.2.5. DNA binding analysis using viscosity measurement

The hydrodynamic method (viscometric measurement) is also a crucial tool to find the nature of binding of metal complexes to the

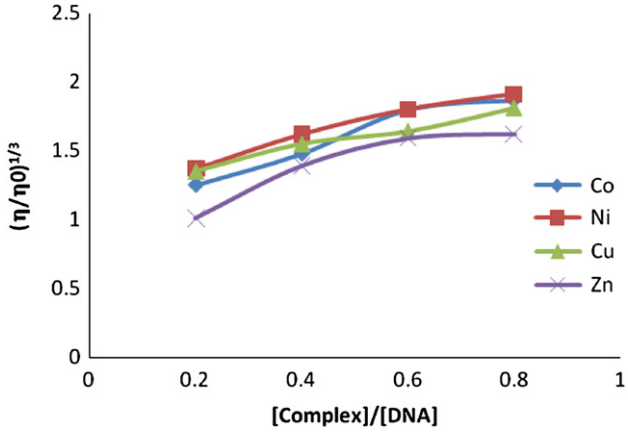


**Fig. 5.** Effects of increasing amounts of Co-complex, Ni-complex, Cu-complex and Zn-complex on the relative viscosities of *E. coli* DNA at 29 °C.

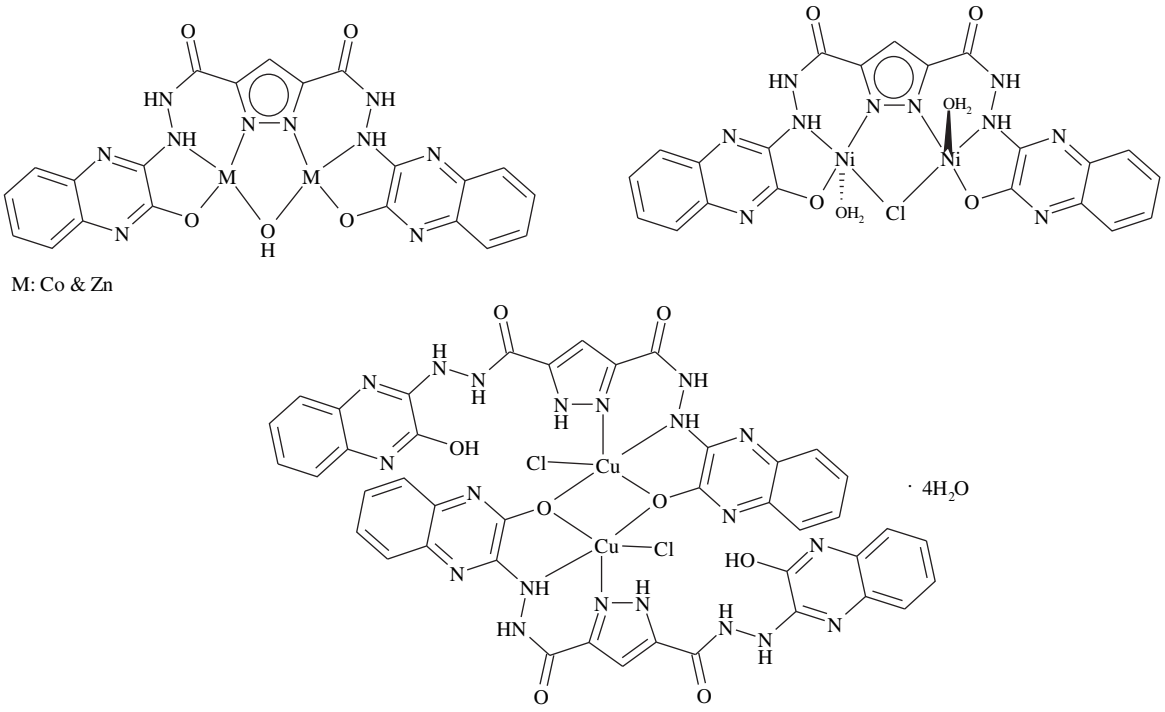


**Fig. 6.** Proposed structures of the complexes.

DNA, in which the solution viscosity of DNA is sensitive to the changes in the effective length of DNA molecules is one of the most critical tests for inferring the binding mode (intercalation or other binding modes) of DNA. This study was regarded as the least ambiguous and the most critical tests of binding mode in solution state in absence of crystallographic structural data [30–32]. Under the appropriate conditions intercalation causes noteworthy increase in the viscosity of DNA solution due to the disjointing of base pairs at intercalation spots. The results of the viscosity measurements for all the complexes that are bound to DNA show increase in relative viscosities with an

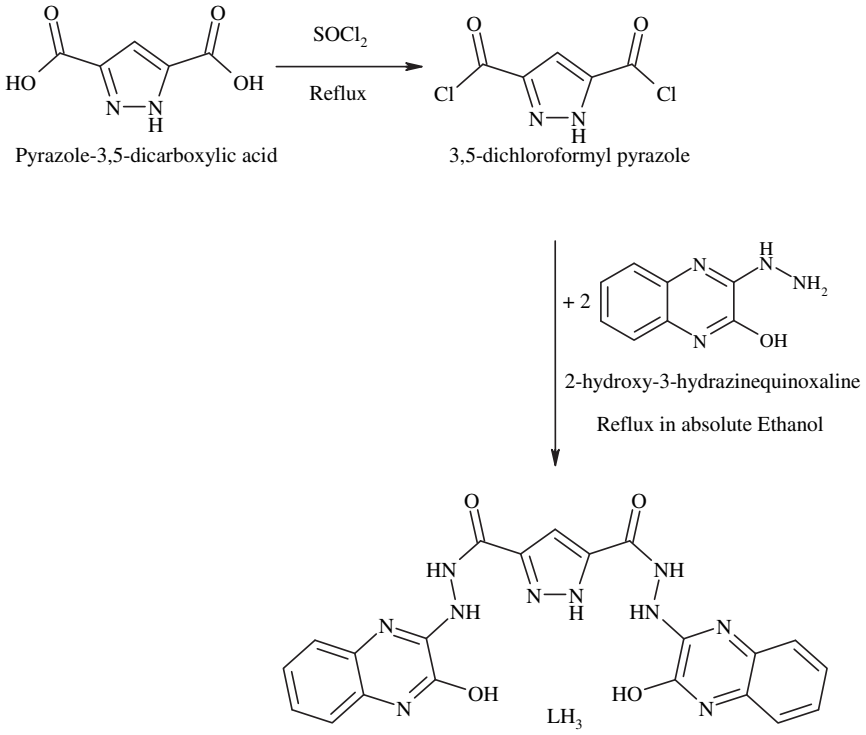


**Fig. 7.** Scheme: preparation of the ligand.

increase in the [complex]/[DNA] ratio (where [complex] is 50, 100, 150 and 200 μl) as shown in Fig. 5. Thus, the increase in the viscosity has been attributed to the enlargement of the separation between base pairs, which are pushed apart to accommodate the intercalating molecule [33–35]. These results suggested an intercalative binding mode of the complexes with DNA and also hold up the results obtained from electronic absorption studies.

## 3. Conclusion

It is concluded from analytical and spectral data that, the ligand acts as tridentate monobasic and hexadentate tribasic chelate with donating sites $N_2O$ and $N_4O_2$ respectively. Electronic and magnetic moment data support the square pyramidal geometry around copper and nickel metal ions, whereas cobalt is tetrahedral. Zinc complex is found to be tetrahedral and copper complex is mononucleating and dimeric in nature, which are confirmed by the spectral and elemental analysis (Fig. 6). ESR spectrum of copper complex shows line broadening due to bulkier organic ligand and magnetic moment confirms the weak antiferromagnetic interaction between copper centers. Anti-biogram studies witnessed the prominent activity of copper complex with compared to the activity of tested compounds. The DNA binding experiments using electronic spectral technique show the hypochromism at d–d transition region and hypochromism and red shift at the charge transfer region. Viscosity measurement confirms the intercalative binding mode of complexes with the *E. coli* DNA. The same is further witnessed by the DNA melting temperature studies.

## 4. Experimental protocol

All the chemicals used were of reagent grade and the solvents were dried and distilled before use according to the standard procedures. The preparation of 2-hydroxy-3-hydrazino quinoxaline was prepared according to the earlier reports [36] and pyrazole-3,5-dicarboxylic acid was purchased. The metal chlorides used were in the hydrated form. All the compounds were analyzed for Carbon, Hydrogen and Nitrogen by Thermo quest elemental analyzer. Estimation of the metal(II) ions was done according to the standard methods. The molar conductivity measurements were made on ELICO-CM-82 conductivity bridge. The magnetic susceptibility measurements were made on Faraday balance at room temperature using $Hg[Co(SCN)_4]$ as calibrant. The $^1H$ NMR spectra were recorded in DMSO-$d_6$ solvent on Bruker-300 MHz spectrometer at room temperature using TMS as internal reference. IR spectra were recorded in a KBr matrix using an Impact-410 Nicolet (USA) FT-IR spectrometer in 4000–400 $cm^{-1}$ range. The electronic spectra of the complexes were recorded on a Hitachi 150–20 spectrophotometer in the range of 1000–200 nm. The cyclic voltammetric studies were performed at room temperature in DMSO under $O_2$ free condition using CH instruments Electrochemical analyzer, CHI-1110 A (USA). The ESR spectra of the copper complexes were scanned on a Varian E-4X-band EPR spectrometer, using TCNE as the g-marker. TG and DTA measurements of the complexes were recorded in nitrogen atmosphere on Universal V2.4F TA Instrument keeping final temperature at 800 °C and heating rate was 10 °C/min. The FAB mass spectra were drawn from JEOL SX 102/DA-6000 mass spectrometer using Argon/Xenon (6 kV, 10 mA) as the FAB gas.

### 4.1. Chemistry

#### 4.1.1. Preparation of the ligand ($LH_3$)

Pyrazole-3,5-dicarboxylic acid (0.02 M) was refluxed with 10 ml of thionyl chloride for about 4 hrs at 110–115 °C under anhydrous conditions. Excess thionyl chloride was removed under reduced pressure. The resultant white pasty solid was cooled in an ice bath for about 15 min and the hot ethanolic solution of 2-hydroxy-3-hydrazinequinoxaline (0.04 M) was added and further refluxed for about 4 h, where upon a clear pale yellow solution was produced. The resultant solution was then cooled to get the yellow colored ligand ($LH_3$) (Fig. 7), which was separated by filtration under suction and dried under lamp. The ligand is recrystallized from hot ethanol. Yield: 78%, M.P.: >300 °C.

#### 4.1.2. Preparation of complexes

The complexes of the ligand $LH_3$ viz., $Co^{II}$, $Ni^{II}$, $Cu^{II}$ and $Zn^{II}$ were prepared by refluxing the respective metal chlorides (0.002 mol) in 50 ml of ethanol with ligand (0.001 mol) for about 3–4 h at water bath temperature. In case of cobalt and nickel complexes the pH of the solution was raised by the addition of alcoholic $NH_3$ in order to separate the complexes in solid form. So obtained complexes were filtered under suction and dried over anhydrous $CaCl_2$.

### 4.2. Biochemistry

#### 4.2.1. Methodology for anti-biogram analysis against bacteria

*Media Used*: Peptone-10 g, NaCl-10 g and Yeast extract 5 g, Agar 20 g in 1000 ml of distilled water.

Initially, the stock cultures of *E. coli* and *Pseudomonas* were revived by inoculating in broth media and grown at 37 °C for 18 h. The agar plates of the above media were prepared and wells were made in the plate. Each plate was inoculated with 18 h old cultures (150 μl) and spread evenly on the plate. After 20 min, the wells were filled with 100 μl of each compound (10 mg/ml in DMF). The control plates with Gentamycin (10 mg/ml) and DMF were also prepared. All the plates were incubated at 37 °C for 24 h and the diameter of inhibition zone was noted. The values were compared with that of Gentamycine and the samples showing significant inhibition were selected for the further calculation of minimum inhibition concentration (MIC).

The MIC of compounds was determined by assaying at 500 and 250 μg concentrations along with standard gentamycin at the same concentrations. The cultures were grown for 24 h and the zones were compared with that of gentamycin and % of inhibition was calculated.

#### 4.2.2. Methodology for anti-biogram analysis against fungi

*Media Used*: Potato Dextrose Agar (PDA). 250 g of peeled potato were boiled for 20 min and squeezed and filtered. To this filtrate 20 g of dextrose was added and the volume was made up to 1000 ml by distilled water.

Initially, the stock cultures of *A. niger* and *Cladosporium* were revived by inoculating in broth media and grown at 37 °C for 48 h. The agar plates of the above media were prepared and wells were made in the plate. Each plate was inoculated with 48 h old cultures (150 μl) and spread evenly on the plate. After 20 min, the wells were filled with 500 μl of each compound (10 mg/ml in DMF). The control plates with Flucanazole (10 mg/ml) and DMF were also prepared. All the plates were incubated at 37 °C for 48 h and the diameter of inhibition zone was noted. The values were compared with that of flucanazole and the samples showing significant inhibition were selected for the further calculation of MIC.

The MIC of compounds was determined by assaying at 500 and 250 μg concentrations along with standard flucanazole at the same concentrations. The cultures were grown for 48 h and the zones were compared with that of flucanazole and % of inhibition was calculated.

#### 4.2.3. Methodology for DNA cleavage analysis

*Culture media*: potato dextrose broth (Peptone 10, NaCl 10 and yeast extract 5 g/l) was used for the growth of the *E. coli*. The 50 ml

media was prepared, autoclaved for 15 min at 121 °C, 15 lb pressure. The autoclaved media were inoculated with the seed culture and incubated at 37 °C for 24 h.

*Isolation of DNA*: DNA was isolated using the procedure mentioned below,

The fresh bacterial culture (1.5 ml) was centrifuged to obtain the pellet and made to dissolve in 0.5 ml of lysis buffer (100 mM tris pH 8.0, 50 mM EDTA, 50 mM lysozyme) and to which added 0.5 ml of saturated phenol followed by the incubation at 55 °C for 10 min. The resultant mixture was centrifuged at 10,000 rpm for 10 min and to the supernatant, equal volume of chloroform and isoamyl alcohol (24.1) and 1/20th volume of 3 M sodium acetate (pH 4.8) were added and further, centrifuged at the same conditions. Soon after, 3 volumes of chilled absolute alcohol were added and so obtained DNA was separated by centrifugation. Finally the pellet was dried and dissolved in TE buffer (10 mM tris pH 8.0, 1 mM EDTA) and stored in cool.

*Sample preparation*: The samples (10 mg/ml) were prepared in DMSO.

*Treatment of DNA with the samples*: The synthetic compounds (100 μg) were added separately to the DNA sample of *E. coli*. The sample mixtures were incubated at 37 °C for 2 h.

*Agarose gel-electrophoresis*: To know the DNA cleavage action of compounds, 200 mg of agarose was dissolved in 25 ml of TAE buffer (4.84 g Tris base, pH 8.0, 0.5 M EDTA/1 L) by boiling and poured into the gel cassette fitted with a comb. When the gel attained ~55 °C, allowed to solidify and then, comb was removed carefully. So obtained solid gel was placed in the electrophoresis chamber flooded with TAE buffer. Subsequently 20 μL of DNA sample (mixed with bromophenol blue dye at 1:1 ratio) was loaded carefully into the wells, along with standard DNA marker and the constant 50 V of electricity was made to pass for around 30 min. Finally, the gel was removed carefully and stained with ETBR (Ethidium bromide) solution (10 μg/ml) for 10–15 min and the bands were observed under UV transilluminator. The illuminated gel was photographed by using a polaroid camera (a red filter and polaroid film were used).

#### 4.2.4. Methodology for DNA binding analysis using electronic spectral method

The concentration of *E. coli* DNA per nucleotide [C(p)] was measured by using its known extinction coefficient at 260 nm (6600 $M^{-1}\,cm^{-1}$) [30]. The absorbance at 260 nm (A260) and at 280 nm (A280) for *E. coli* DNA was measured to check its purity. The ratio A260/A280 was found to be 2.22, indicating that *E. coli* DNA is satisfactorily free from protein. Buffer [5 mM tris(hydroxymethyl) aminomethane, pH 7.2, 50 mM EDTA] was used for the absorption, viscosity, and thermal denaturation experiments.

In absorption studies the complex was dissolved in DMSO to get the desired concentration. The spectroscopic titrations were carried out by adding increasing amounts (20 μl, 40 μl, 60 μl, 80 μl and 100 μl) of *E. coli* DNA to a solution of the complex at a fixed concentration contained in a quartz cell. The UV–Vis spectra were recorded after equilibration at 20 °C for 10 min after each addition. The intrinsic binding constant $K_b$ was determined from the plot of [DNA]/($\varepsilon_a - \varepsilon_f$) vs. [DNA] according to equation (1).

$$[DNA]/(\varepsilon_a - \varepsilon_f) = [DNA]/(\varepsilon_b - \varepsilon_f) + 1/\left[K_b(\varepsilon_b - \varepsilon_f)\right] \quad (1)$$

where [DNA] is the concentration of DNA in base pairs, the apparent absorption coefficients $\varepsilon_a$, $\varepsilon_f$ and $\varepsilon_b$ correspond to *A*obs/[complex], extinction coefficient for the free complex and the extinction coefficient of the complex in the totally bound form, respectively. The data were fitted to Eq. (1), with a slope equal to $1/(\varepsilon_b - \varepsilon_f)$ and *y*-intercept equal to $1/[K\,(\varepsilon_b - \varepsilon_f)]$ and $K_b$ was obtained from the ratio of the slope to the intercept.

#### 4.2.5. Methodology for DNA binding analysis using viscosity measurement

Viscosity measurements were carried out using an *Oswald microviscometer*, maintained at constant temperature (29 °C) in a thermostat. The DNA concentration was kept constant in all samples, but the complex concentration was increased each time (from 50 to 250 mM). Mixing of the solution was achieved by bubbling the nitrogen gas through viscometer. The mixture was left for 10 min at 29 °C after addition of each aliquot of complex. The flow time was measured with a digital stopwatch. The experiment was repeated in triplicate to get the concurrent values. Data are presented as $(\eta/\eta_0)^{1/3}$ versus the ratio [complex]/[DNA], where $\eta$ and $\eta_0$ are the specific viscosity of DNA in presence and in absence of the complex respectively. The values of $\eta$ and $\eta_0$ were calculated by using equation (2),

$$\eta = (t - t_b)/t_b \quad (2)$$

where $t_b$ is the observed flow time of DNA containing solution and, t is the flow time of buffer alone. Relative viscosities for DNA were calculated from the relation $(\eta/\eta_0)$.

#### 4.2.6. Methodology for thermal denaturation study

Thermal denaturation studies were carried out on UV–visible spectrometer, equipped with temperature controlling thermostat. The melting curves ($T_m$) of both free *E. coli* DNA and *E. coli* DNA bound complexes were obtained by measuring the hyperchromicity of *E. coli* DNA at 260 nm as a function of temperature. The melting temperatures were measured in 50 μM DNA in the same buffer at pH 7.2. The temperature was scanned from 25 to 80 °C at a speed of 5 °C per min. The melting temperature ($T_m$) was taken as the mid-point of the hyperchromic transition.

## Acknowledgments

The authors thank the USIC, Karnatak University, Dharwad for providing spectral facility. Recording of FAB mass spectra (CDRI Lucknow) and ESR spectra (IIT Bombay) are gratefully acknowledged. The authors thank (Srinivasa Budagumpi) University Grants Commission, New Delhi, India for awarding Research Fellowship in Science for Meritorious Students and Karnatak University, Dharwad, Karnataka, India (Naveen V. Kulkarni and Sathisha M.P.) for providing research fellowships.

## References

[1] (a) S. Komeda, M. Lutz, L.A. Spek, Y. Yamanaka, T. Sato, S. Chikuma, J. Reedijk, J. Am. Chem. Soc. 124 (2002) 4738–4746;
(b) Y. Xia, C.-D. Fan, B.-X. Zhao, J. Zhao, D.-S. Shin, J.-Y. Miao, Eur. J. Med. Chem. 43 (2008) 2347–2353.
[2] C. Chopard, C. Lenoir, S. Rizzato, M. Vidal, J. Arpalahti, L. Gabison, A. Albinati, C. Garbay, J. Kozelka, Inorg. Chem. 47 (2008) 9701–9705.
[3] F. Caruso, C. Pettinari, F. Marchetti, P. Natanti, C. Phillips, J. Tanski, M. Rossi, Inorg. Chem. 46 (2007) 7553–7560.
[4] A. Prokofieva, I. Alexander, P.S. Dechert, F. Meyer, Chem. Commun. (2008) 1005–1007.
[5] J. Klingele, I. Alexander, P. Guido Leibeling, S. Demeshko, S. Dechert, F. Meyer, J. Chem. Soc. Dalton Trans. (2007) 2003–2013.
[6] A.L. Gavrilova, B. Bosnich, Chem. Rev. 104 (2004) 349–384.
[7] (a) M. Abid, A.R. Bhat, F. Athar, A. Azam, Eur. J. Med. Chem. 44 (2009) 417–425;
(b) F. Meyer, A. Jacobi, B. Nuber, P. Rutsch, L. Zsolnai, Inorg. Chem. 37 (1998) 1213–1218.
[8] (a) R.A. Bhat, F. Athar, A. Azam, Eur. J. Med. Chem. 44 (2009) 426–431;
(b) J.A. Vincent, K. Manoj, M. Jose, L. Laurent, N. Pilar, G.–E. Enrique, A.R. Jose, V.L. Santiago, E. Beatriz, J. Org. Chem. 64 (1999) 6135–6146.
[9] L.J. Bellamy, The Infrared Spectra of Complex Molecules, third ed. Methuen, London, 1954.
[10] V.H. Arali, V.K. Revankar, V.B. Mahale, Transition. Met. Chem. 18 (1993) 158–161.
[11] A.D. Naik, S.M. Annigeri, U.B. Gangadharmath, V.K. Revankar, V.B. Mahale, J. Mol. Struct. 616 (2002) 119–127.
[12] (a) S. Budagumpi, M.P. Sathisha, N.V. Kulkarni, G.S. Kurdekar, V.K. Revankar, J. Incl. Phenom. Macrocycl. Chem. (2009) doi:10.1007/s10847-009-9649-z.
(b) S. Sujatha, T.M. Rajendiran, R. Kannappan, R. Venkatesan, P.S. Rao, Proc.

Indian Acad. Sci. (Chem. Sci.) 112 (2000) 559–572;
(c) W. Mazurek, H.M. Bond, K.S. Murray, M.J. O'Conner, A.G. Weed, Inorg. Chem. 24 (1985) 2484–2489.
[13] D.X. West, A.A. Nassar, Transition. Met. Chem. 24 (1999) 617–621.
[14] A.B. P Lever, Inorganic Electronic Spectroscopy. Elsevier, Amsterdam, 1968.
[15] S.K. Sandra, C.R. Blaga, K. Aleksandra, J. Therm. Anal. Cal. 90 (2007) 525–531.
[16] H. Okawa, M. Tadokoro, Y. Aratake, M. Ohba, K. Shindo, M. Mitsumi, M. Tomono, D.E. Fnton, J. Chem. Soc. Dalton Trans. (1993) 253–258.
[17] M. Handa, T. Idehara, K. Nakano, K. Kasuga, M. Mikuriya, N. Matsmoto, M. Kodera, S. Kida, Bull. Chem. Soc. Jpn. 65 (1992) 3241–3252.
[18] A.I. Uraev, V.P. Kurbatov, A.L. Nivorozhkin, L.S. TyÍchenko, V.G. Vlasenko, L.N. Divaeva, K.A. Lyssenko, M.Y. Antipin, A.D. Garnovskii, Russ. Chem. Bull. Int. Edn. 51 (2002) 1924–1927.
[19] M. Ulusoy, H. Karabıyık, R. Kılınc, A.M. Aygün, B. Cetinkaya, S.G. Granda, Struct Chem. 19 (2008) 749–755.
[20] C. Keshavalu, R.S. Naidu, R.R. Naidu, Polyhedron 4 (1985) 761–764.
[21] M.C. Jain, A.K. Srivastava, P.C. Jain, Inorg. Chem. Acta 23 (1977) 199–203.
[22] W.J. Geary, Coord. Chem. Rev. 7 (1971) 81–122.
[23] S.R. Korupoju, N. Mangayarkarasi, S. Ameerunisha, E.J. Valente, P.S. Zacharis, J. Chem. Soc. Dalton Trans. (2000) 2845–2852.
[24] T.M. Kelly, A.B. Tossi, D.J. McConnell, T.C. Strekas, Nucl. Acids Res. 13 (1985) 6017–6034.
[25] J.K. Barton, A.T. Danishefsky, J.M. Goldberg, J. Am. Chem. Soc. 106 (1984) 2172–2176.
[26] S.A. Tysoe, R.J. Morgan, A.D. Baker, T.C. Strekas, J. Phys. Chem. 97 (1993) 1707–1711.
[27] J.M. Kelly, A.B. Tossi, D.J. McConnell, C. Ohuigin, Nucl. Acids Res. 13 (1985) 6017–6034.
[28] S. Murali, C.V. Sastri, B.G. Maiya, Proc. Indian Acad. Sci. (Chem. Sci.) 114 (2002) 403–415.
[29] R.B. Ĺopez, B.L. Loeb, T. Boussie, T.J. Meyer, Tetrahedron. Lett. 37 (1996) 5437–5440.
[30] S. Zhang, Y. Zhu, C. Tu, H. Wei, Z. Yang, L. Lin, J. Ding, J. Zhang, Z. Guo, J. Inorg. Biochem. 98 (2004) 2099–2106.
[31] V.A. Izumrudov, M.V. Zhiryakova, A.A. Goulko, Langmuir 18 (2002) 10348–10356.
[32] J. Liu, T. Zhang, T. Lu, L. Qu, H. Zhou, Q. Zhang, L. Ji, J. Inorg. Biochem. 91 (2002) 269–276.
[33] S. Satyanarayana, J.C. Dabrowiak, J.B. Chaires, Biochemistry 31 (1992) 9319–9324.
[34] R. Rao, A.K. Patra, P.R. Chetana, Polyhedron 27 (2008) 1343–1352.
[35] Q.-X. Wang, K. Jiao, F.-Q. Liu, X.-L. Yuan, W. Sun, J. Biochem. Biophys. Methods 70 (2007) 427–433.
[36] S.M. Annigeri, M.P. Sathisha, V.K. Revankar, Transition. Met. Chem. 32 (2007) 81–87 (And the references therein).